Shape From Symmetry

Sebastian Thrun
Stanford University and Strider Labs
353 Serra Mall, Stanford, CA 54305
Email: thrun@stanford.edu

Ben Wegbreit
Strider Labs
1516 Dana Street, Palo Alto, CA 94303
Email: benw@striderlabs.com

Abstract

We describe a technique for reconstructing probable occluded surfaces from 3-D range images. The technique exploits the fact that many objects possess shape symmetries that can be recognized even from partial 3-D views. Our approach identifies probable symmetries and uses them to extend the partial 3-D shape model into the occluded space. To accommodate objects consisting of multiple parts, we describe a technique for segmenting objects into parts characterized by different symmetries. Results are provided for a real-world database of 3-D range images of common objects, acquired through an active stereo rig.

1. Introduction

In recent years, shape completion has become a major research area in 3-D computer vision. In the shape completion problem, one is given a partial 3-D view of an object surface. The view might be acquired through a stereoscopic camera system, a laser-based range finder, or similar. The view only captures one side of the object; other surfaces remain occluded. The shape completion problem is the problem of reconstructing these occluded surfaces from the visible parts of the object.

The problem of shape recovery has been addressed in a number of papers. Some techniques infer 3-D structure from 2-D images, exploiting cues such as corner geometry [6], vanishing points [3], shading [4], mirror images [10], even fog [11]. Techniques for shape estimation from multiple images are commonly known as structure from motion [13, 17]; however, reconstructing *occluded* surfaces is rarely addressed in 2-D computer vision. For 3-D views of an object, which is the problem addressed here, reconstruction is usually performed through the iterated closest point (ICP) algorithm [1]. This algorithm requires multiple views and is unable to reconstruct invisible surfaces. By registering partial 3-D views to a database of known objects the occluded surface can indeed be reconstructed [5], but at the time of database construction the occluded surfaces must be visible.

This paper proposes the use of symmetry for probable shape reconstruction. As argued in [8], many man-made and natural objects are symmetric, or possess parts that are symmetric [14]. Examples of approximately-symmetric objects include books (plane reflection symmetry), bagels (axial symmetry paired with a plane reflection symmetry), and oranges (spherical symmetry). Even if an object is not globally symmetric, parts of it may be. For example, a tree is usually not symmetric, but many of its branches are approximately axial symmetric.

Symmetry can often be determined even from a partial 3-D view. When a symmetry is found, it allows us to reflect the visible surfaces into the occluded space, thereby predicting shape that is invisible to the imaging device. Naturally, this approach is only applicable if an object is indeed symmetric; and it is only useful if the symmetry does more than just matching visible points to other visible points.

This paper proposes a technique for identifying potential symmetries of objects or object parts. Our approach bases the search for symmetries on a hierarchical generate-and-test procedure, which interleaves search in the space of symmetry types with a search for specific parameters of a symmetry. It exploits a taxonomy of different types of symmetries, which establishes a partial entailment relationship between them. Our approach also segments the partial view into subregions characterized by different symmetries, thereby accommodating objects composed of parts adhering to different, local symmetries.

Experiments with a database of 3-D object views illustrate that in many cases, our approach recovers the complete object shape even from a single 3-D view. The data is acquired by an active stereo rig similar to the one in [15]. In one of our examples, our approach correctly segments a complex puppet into 9 parts all characterized by different local symmetries, thereby reconstructing nearly all of the occluded surfaces. Towards the end of this chapter, we discuss related work on using symmetries in computer vision.

Proceedings of the Tenth IEEE International Conference on Computer Vision (ICCV'05)
1550-5499/05 $20.00 © 2005 **IEEE**

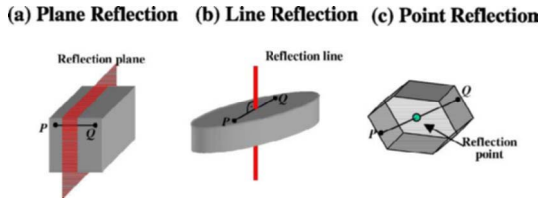

Figure 1. Reflection symmetries.

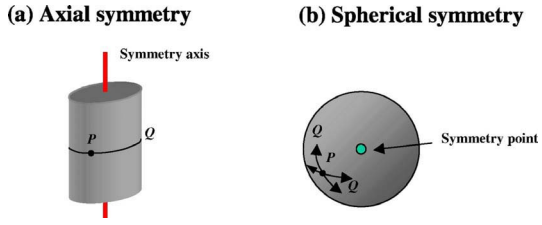

Figure 2. Axial and spherical symmetries.

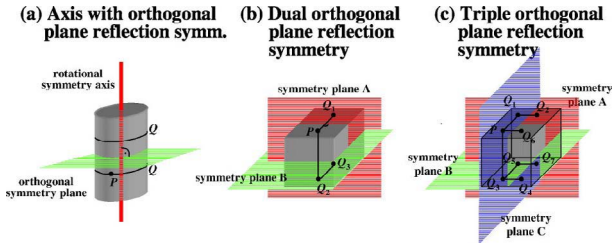

Figure 3. Composite symmetries, constructed from multiple elemental symmetries.

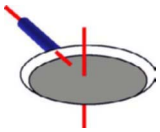

Figure 4. Part symmetries: This idealized frying pan possesses two local axial symmetries.

2. 3-D Symmetries

2.1. Elemental Symmetries

We being with a definition of the types of symmetries considered in this paper; there will be eight symmetries in total. Much of the material in this chapter can be found in basic textbooks on 3-D geometry and topology [14, 21].

We begin our consideration with the definition of the term *symmetry feature*. In $\Re^3$ there exist three basic symmetry features: a *plane*, an *axis*, and a *point*. Each of these features establish equivalence classes of multiple surface points. We also distinguish *reflection*, *axial*, and *spherical* symmetries.

In detail, a *reflection symmetry* associated each point P on the object surface to another surface point Q on the opposite side of the object. The definition of "opposite" is a function of the symmetry feature. For example, a *plane reflection symmetry* reflects points to the opposite side of the symmetry plane. This is illustrated in Fig. 1a, which shows an object with an associated symmetry plane, along with an example point P and the reflected point Q. A *reflection line* reflects points across a line. Fig. 1b illustrates such a reflection line, which reflects a point P to a reflection point Q on the opposite side of the line. Likewise, a *reflection point* reflects a point P to the opposite side of side of the point, as illustrated in Fig. 1c. All three reflection symmetries associate exactly one reflected point Q with each point P on the surface.

Axis/spherical symmetries associate entire manifolds, or point sets, $\mathcal{Q} = \{Q\}$ with each surface point P (in the non-degenerate case). Consider, for example, an axial symmetry, illustrated in Fig. 2a. The axial symmetry associates each point P with an entire circle of points $\mathcal{Q}$, which includes P. The center of the circle intersects with the symmetry axis. The embedding plane of the circle is orthogonal to this axis.

Spherical symmetries reflect each point P on the object surface to an entire sphere, whose center is the symmetry point. Figure 2b illustrates a spherical symmetry.

2.2. Composite Symmetries

Composite Symmetries are defined through two or more basic symmetries. For example, objects may possess three orthogonal plane reflection symmetries, such as the cube shown in Fig. 3c. Such a combination of three orthogonal reflection planes shall be considered a composite symmetry. It maps each point P to a total of seven other points on the object surface, in that there exist $2^3 - 1 = 7$ different combinations of invoking one or more plane reflection symmetries.

We consider three different composite symmetries, induced by the following symmetry features: *dual orthogonal reflection planes*, *triple orthogonal reflection planes*, and *a axial symmetry combined with an orthogonal reflection plane*. These symmetries are illustrated in Fig. 3. Specifically, a cylinder is not only axial-symmetric, but also plane reflection-symmetric as illustrated in Fig. 3a. Thus, each point P is reflected into two circles on the object (in the non-degenerate case). The analogous cases of multiple orthogonal reflection planes are shown in Fig. 3b&c.

We note that the list of symmetries considered here is by no means complete; see [14] for further discussion. Our choice of symmetry types has been restricted to some of the most common symmetries found in natural environments.

2.3. The Entailment Hierarchy

A key property of the symmetries discussed thus far is that they establish a natural *entailment hierarchy*. This entailment hierarchy will prove essential for the design of a fast, global search algorithm.

The hierarchy is based on the observation that certain symmetries imply other, weaker symmetries. For example,

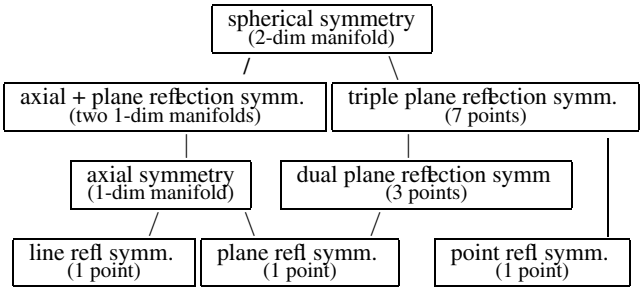

Figure 5. The entailment hierarchy of symmetries. This hierarchy establishes a half order of entailment of different symmetry types. This diagram also lists the number of reflection points for each point P under the respective symmetry.

any object that is spherically symmetric is also axial symmetric, and the axis might be defined arbitrarily as long as it contains the spherical symmetry point. Likewise, any axial symmetrical object is also plane reflection symmetric, for any reflection plane that fully contains the symmetry axis. This insight shall allow us to organize our search for possible symmetries in stages; for example, failure to find a plane reflection symmetry immediately implies that the object may not be axial symmetric! This renders the entailment hierarchy a powerful tool in discovering symmetries.

Fig. 5 shows the entailment hierarchy for the eight symmetries considered in this paper. The hierarchy constitutes a half-order, as there exist symmetries whose absence or presence is unrelated to other symmetries. This diagram also lists the number of reflection points Q for each point P under the respective symmetry—which ranges from a single point for the various reflection symmetries, all the way to a 2-dimensional manifold for the spherical symmetry. The space of reflected points $\mathcal{Q}$ increases as we upward-transcend the hierarchy.

3. Reflecting Visible Points

To discuss our symmetry search algorithm, we need to define the mathematics of reflecting a point. Let P be a surface point, usually a point in a partial 3-D view of an object.

- A reflection plane reflects P to a single reflected point Q. If we assume the plane is defined through a normal n and a scalar distance β of the plane from the origin, the point Q is computed as follows:

$$Q \;=\; P - 2n\,(P^T\,n - \beta) \tag{1}$$

  The term in squared brackets is the distance of P to the reflection plane. The subtraction of $2n$ times this distance reflects the point to the other side of the plane.
- A symmetry axis is defined through a normal n and a point a. The normal defines a rotation matrix R, as a solution to the following implicit equation:

$$n \;=\; R \begin{pmatrix} 0 \\ 0 \\ 1 \end{pmatrix} \tag{2}$$

  To rotate a point P about this axis by angle α, we map it into the local coordinate system of the axis, rotate it, and then map it back into the original coordinate system:

$$Q(\alpha) \;=\; R^T \begin{pmatrix} \cos\alpha & \sin\alpha & 0 \\ -\sin\alpha & \cos\alpha & 0 \\ 0 & 0 & 1 \end{pmatrix} R(P-a) + a \tag{3}$$

  The resulting set $\mathcal{Q} = \{Q(\alpha)\}$ is a 1-D manifold that corresponds to the surface point under the axial symmetry.
- A line reflection symmetry is obtained by using $\alpha = \pi$ in the reflective law of the axial symmetry, Eq. 3.
- A spherical symmetry is defined through a symmetry point a. The rotation induces a two-dimensional manifold about a, which is obtained via two nested rotations:

$$Q(\alpha,\gamma) \;=\; \begin{pmatrix} 1 & 0 & 0 \\ 0 & \cos\alpha & \sin\alpha \\ 0 & -\sin\alpha & \cos\alpha \end{pmatrix} \begin{pmatrix} \cos\gamma & 0 & \sin\gamma \\ 0 & 1 & 0 \\ -\sin\gamma & 0 & \cos\gamma \end{pmatrix} (P-a) + a \tag{4}$$

  The set of points $\mathcal{Q} = \{Q(\alpha,\gamma)\}$ is the resulting 2-D manifold of points that corresponds to P under a spherical symmetry.
- A point reflection symmetry is derived from the spherical symmetry using $\alpha = \gamma = \pi$ in Eq. 4

These equations define the five elemental symmetries considered here. The three composite symmetries are defined by reflecting points through all or some of the respective elemental symmetries.

4. Scoring Symmetries

The problem of symmetry identification is the problem of determining which of the symmetries above are characteristic of an observed 3-D point cloud. We begin our consideration with a technique for scoring a hypothetical symmetry.

4.1. Probabilistic Measurement Model

Suppose we hypothesize the existence of a specific symmetry. Our approach evaluates this hypothesis through a probabilistic measurement model, which incorporates models of sensor noise and occlusion.

Specifically, let us denote the set of visible surface points in the 3-D view by $\mathcal{P} = \{P\}$. The observed points cast an

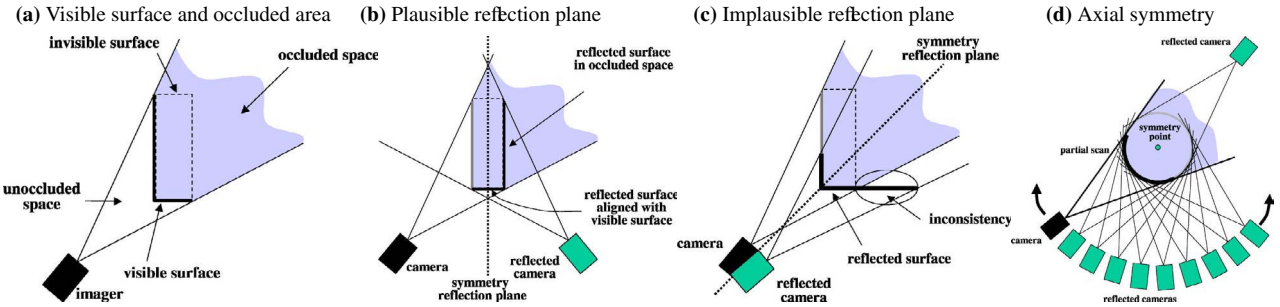

Figure 6. Illustration of visible point clouds, occluded areas, and their utility in distinguishing plausible from implausible symmetries. Panel (c) shows an *implausible* symmetry, which reflects many surface points into unoccluded space.

occlusion shadow, as illustrated by the grayly shaded area in Fig. 6a. When applying a symmetry, the points $\mathcal{P}$ are reflected into another set of points $\mathcal{Q}$, following the equations set forth in the previous section. This is illustrated in Fig. 6b for a reflection plane symmetry. Ideally, every point in $\mathcal{Q}$ should either coincide with a point in $\mathcal{P}$ or fall into the occluded space (shown in gray in Fig. 6b). Points in $\mathcal{Q}$ that coincide with $\mathcal{P}$ *confirm* a symmetry; points in the occluded space provide new surface information not existent in the original 3-D view. Points may also fall into the *unoccluded* space. This is illustrated in Fig. 6c, which shows a different (false!) reflection symmetry. The points circled by the ellipse fall into the unoccluded space relative to the original scan, hence should have been visible! Such points contradict a hypothetical symmetry.

To account for the measurement noise in the measurement process, we rely on a probabilistic measurement model. Consider a point $Q \in \mathcal{Q}$. The probability that Q was generated by the visible surface $\mathcal{P}$ is assumed to be Gaussian:

$$p(Q \mid \mathcal{P}, \text{match}) \;=\; \underset{P \in \mathcal{P}}{\text{argmax}} \; |2\pi\Sigma_{\text{match}}|^{-\frac{1}{2}} \; \exp -\tfrac{1}{2}(Q-P)^T \; \Sigma_{\text{match}}^{-1} \; (Q-P) \tag{5}$$

Here "match" specifies the cause of a measurement (correspondence) and Σ_{match} is a noise covariance.

To model occlusion, we consider the points $\bar{\mathcal{P}}$ as the set of occluded points. We define a similar Gaussian distribution to the one above, but over the nearest neighbor in the occluded space:

$$p(Q \mid \mathcal{P}, \text{occl}) \;=\; \underset{\bar{P} \in \bar{\mathcal{P}}}{\text{argmax}} \; |2\pi\Sigma_{\text{occl}}|^{-\frac{1}{2}} \; \exp -\tfrac{1}{2}(Q-\bar{P})^T \; \Sigma_{\text{occl}}^{-1} \; (Q-\bar{P}) \tag{6}$$

Here Σ_{occl} is a different covariance. Notice that the maximization is performed over points $\bar{P}$ in the occluded space. This maximization is easily implemented using ray casting.

Finally, our model allows for "stray" points, through the following distribution:

$$p(Q \mid \mathcal{P}, \text{random}) \;=\; \eta \tag{7}$$

Here η is a constant (defined by the inverse of the maximum measurement range).

All three of components of this probabilistic model are combined into a single measurement probability via Bayes rule:

$$\begin{aligned} & p(Q \mid \mathcal{P}) \\ &= \; p(\text{match})\; p(Q \mid \mathcal{P}, c = \text{match}) \\ &\quad + p(\text{occl})\; p(Q \mid \mathcal{P}, c = \text{occl}) \\ &\quad + p(\text{random})\; p(Q \mid \mathcal{P}, c = \text{random}) \end{aligned} \tag{8}$$

with $p(\text{match}) + p(\text{occl}) + p(\text{random}) = 1$. We approximate the logarithm of this model using Jensen:

$$\begin{aligned} & -\log p(Q \mid \mathcal{P}) \\ &\approx \; -p(\text{match})\; \log p(Q \mid \mathcal{P}, c = \text{match}) \\ &\quad - p(\text{occl})\; \log p(Q \mid \mathcal{P}, c = \text{occl}) \\ &\quad - p(\text{random})\; \log p(Q \mid \mathcal{P}, c = \text{random}) \\ &= \; \text{const.} + \frac{1}{2} \\ &\quad \Big[p(\text{match})\; \underset{P \in \mathcal{P}}{\text{argmax}} (Q-P)^T \; \Sigma_{\text{match}}^{-1} \; (Q-P) \\ &\quad + p(\text{occl})\; \underset{\bar{P} \in \bar{\mathcal{P}}}{\text{argmax}} (Q-\bar{P})^T \; \Sigma_{\text{occl}}^{-1} \; (Q-\bar{P}) \\ &\quad + p(\text{random})\; \log \eta \Big] \end{aligned} \tag{9, 10}$$

This conditional probability is quite interesting. The first term in the squared brackets is the quadratic surface distance familiar from ICP [1]. The third term extends this to (the negative logarithm of) a "Gaussian with heavy tails," by bounding from below the quadratic function by a positive constant. The middle models occlusion. It allows for points to be reflected into occluded space by a hypothetical symmetry. This part of the measurement model is essential for surface completion in that points that are reflected into occluded space extend the visible 3-D surface.

4.2. Scoring A Symmetry

The measurement model provides us with a method to "score" a point Q generated by a symmetry. The total score

of a symmetry is obtained by

$$-\log p(\mathcal{Q} \mid \mathcal{P}) \quad = \quad -\frac{1}{|\mathcal{Q}|} \sum_{Q \in \mathcal{Q}} \log p(Q \mid \mathcal{P}) \qquad (11)$$

This formula is derived by assuming conditional independence, and by normalizing for the size of the point set $\mathcal{Q}$. For symmetries that induce a continuum over points, our approach samples from this continuum, as illustrated in Fig. 6d.

5. Search in Symmetry Space

A symmetry is defined by three components: a symmetry type of the eight types defined in Fig. 5; a symmetry parameter vector; and a symmetry domain, which specifies the points in the partial view to which the symmetry applies.

The search for a valid set of symmetries is achieved by a triple nested loop. At the outer loop, our approach searches for appropriate symmetry types. For each such type, the middle loop identifies an appropriate symmetry domain. The inner loop determines the parameters of the symmetry feature. We begin with the inner loop.

5.1. Searching Symmetry Parameters

Given a symmetry type and a domain, the inner loop determines the optimal symmetry parameters.

Our search proceeds in two phases: a global parameter search, followed by a local hill climbing search. For reasons that will become obvious below, the global searches involve between one and four parameters (even though certain symmetries are defined through more than four parameters). The set of symmetry parameters is first searched over a discrete grid. For each possible setting of those parameters, the points $\mathcal{P}$ that fall into the domain are reflected into a set of points $\mathcal{Q}$. We then apply the scoring technique described in the previous section to evaluate the parameter vector. The resulting hypercube is searched for local minima of the scoring function. Those are assembled into a list.

Subsequently, each entry on the list is optimized via hill climbing in the parameter space, so as to further improve the score. The resulting set of scored parameters is then pruned to eliminate identical parameter vector, and then thresholded. Parameter vectors whose score fall below the threshold are retained; all other parameter vectors are discarded.

The result of this search is a set of acceptable symmetry parameters. If this set is empty, the symmetry type as whole is judged to be inapplicable for the domain of points chosen.

5.2. Searching Symmetry Types

In the outer loop, our approach searches for applicable symmetry types. We can limit the amount of search necessary through three observations:

```
search plane reflection symmetry (3-D search)
if search succeeded
  search axial symmetry (2-D search)
  if search succeeded
    search spherical symmetry (1-D search)
    if search succeeded
      return spherical symmetry
    else
      search axial symmetry with orthogonal reflection
                                  plane symmetry (1-D search)
    if search succeeded
      return axial+reflection plane symmetry
    else
      return previously found axial symmetry
  else search dual plane reflection symmetry (2-D search)
    if search succeeded
      search triple plane reflection symmetry (1-D search)
      if search succeeded
        return triple plane reflection symmetry
      else
        return previously found dual plane reflection symmetry
  else
    return previously found reflection plane symmetry
else
  search point reflection symmetry (3-D search)
  if search succeeded
    return point reflection symmetry
  else search line reflection symmetry (4-D search)
    if search succeeded
      return line reflection symmetry
return no symmetry
```

Table 1. Algorithm for sequentially searching symmetry types.

- By searching symmetries bottom-up in the entailment hierarchy (Fig. 5), failure to identify a specific symmetry may eliminate an entire set of parent symmetries. For example, failure to find a plane reflection symmetry eliminates five other symmetries (the axial, spherical, and all composite symmetries).
- Lower level symmetries in the entailment hierarchy *constrain* the parameters of higher level symmetry features in this search. For example, we know that the location of a symmetry axis must either be orthogonal or coincide with the plane of a plane reflection symmetry, should the object be at all axial symmetric. Thus, the search of all axes can be constrained accordingly, reducing a potential 4-D search down to a 2-D search. Even more drastic is the transition from an axial to a spherical symmetry. Clearly, any point defining a spherical symmetry must lie on the axis of a previously found axial symmetry. Hence, we can find a spherical symmetry via a 1-D search when seeded with an axial symmetry, instead of a full 3-D search that would be required for searching a spherical symmetry from scratch.
- Some symmetry types are more useful than others with regards to the shape completion problem. For example, a spherical symmetry enables us to map surface points P into two-dimensional manifolds, defined over two free

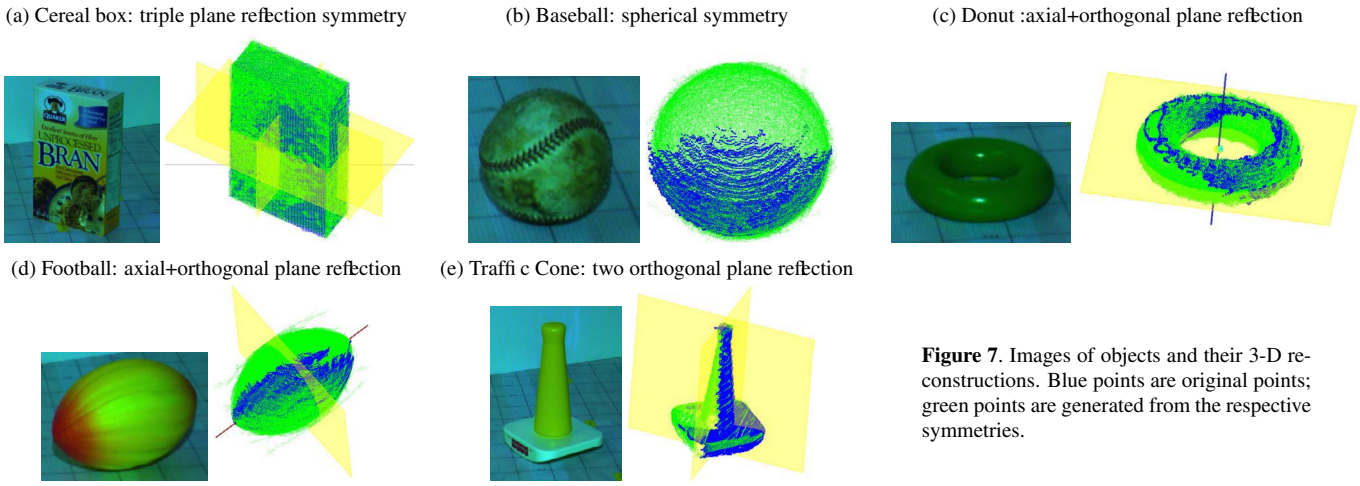

Figure 7. Images of objects and their 3-D reconstructions. Blue points are original points; green points are generated from the respective symmetries.

parameters α and γ. In contrast, each reflection plane symmetry produces only a single point Q. Thus, when a spherical symmetry is found, the search can safely be aborted. The size of the reflected point space establishes yet another hierarchy over all symmetries, which is related to the entailment hierarchy discussed previously.

These observations lead to the nested search algorithm depicted in Tab. 1. It accepts as an input a range scan with associated camera position, and outputs the best found symmetry type and parameters. The dimensionality of the individual symmetry searches is as indicated.

5.3. Searching Symmetry Domains

The final dimension of this work concerns the identification of *local symmetries*, or *part symmetries*. This is the middle loop of our search. Fig. 4 illustrates an object characterized by two axial symmetries, both local to a component of this object.

Finding local symmetries is a segmentation problem. Specifically, our approach associates subsets of points $\mathcal{P}$ with a part symmetry. However, not all such subset are eligible. For a subset to form a legitimate domain, our approach requires that the domain must be contiguous; it domain must meet a minimum size requirement; and it must possess a small rim relative to its interior size.

Unfortunately, the space of all domains is prohibitively large, hence our approach uses heuristics to identify appropriate domains. It starts with the number of points that are not presently "claimed" by another symmetry. From there, it grows the largest connected component to encompass all points that score well under a proposed symmetry. In a final "cleaning step," our approach integrates any point that is entirely enclosed in this set of points, and it also integrates points on the object border that are adjacent to this point set (see [24]).

The result is a contiguous point set that possesses no internal islands, and that tends to possess a small rim relative to its interior size. If this domain meets all criteria stated above, it is used for the nested parameter search.

We note that the search for symmetry parameters and the domain is interleaved in our implementation, to accommodate the effect that the choice of a domain and of a suitable parameter vector are interdependent.

6. Experimental Results

We applied our approach to a number of range images of common household objects. All range images were acquired by an active stereo rig similar to the one described in [15]. To segment the object from the background, the objects were placed on a table. The table coordinates were determined through a planar surface fit, and only the non-table points were used. The resulting point set was analyzed for the largest connected component, and only this component was retained for our analysis.

Fig. 7 shows a number of objects characterized by different types of global symmetries. It also shows our reconstruction of these objects, and lists the types of symmetries found by our algorithm. All of those results are obtained from a single stereoscopic range image per object.

Of particular interest to us is the notion of a part symmetry (local symmetry). Because part symmetries require segmentation, finding such symmetries is significantly more difficult than finding global ones. This is illustrated in Fig. 8. The mug shown there possesses multiple global plane reflection symmetries, as shown in Fig. 8d&e. However, its reconstruction is more complete when identifying the axial symmetry. Unfortunately, the handle violates this axial symmetry; hence, it is a local symmetry.

Our approach finds—fully autonomously—the axial symmetry, along with a segmentation of the object. It then successfully identifies the reflection plane symmetry of its

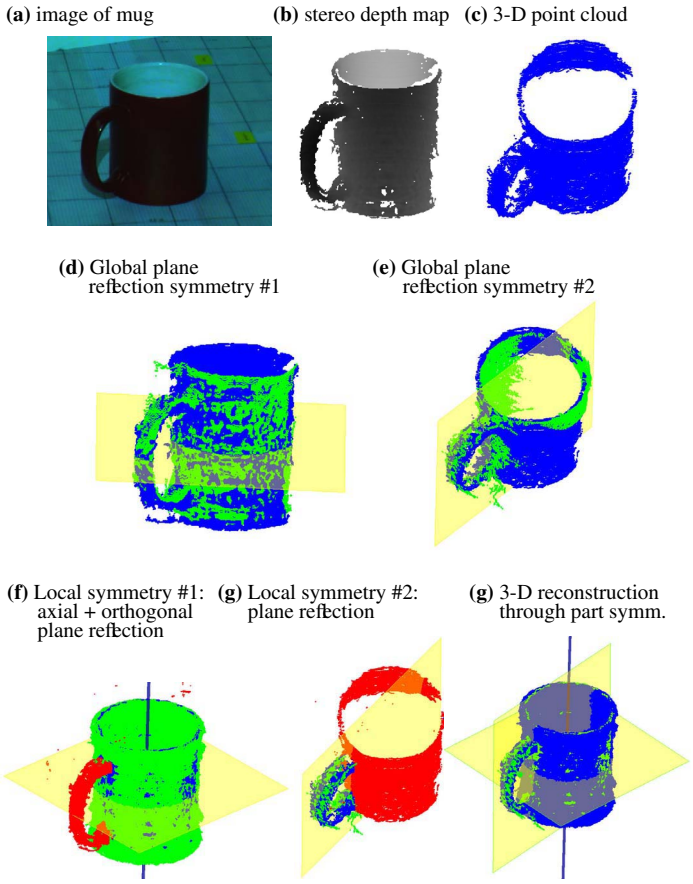

Figure 8. Reconstruction of a mug through local symmetries.

handle. These local symmetries are shown in Fig. 8f&g. Fig. 8h shows the final reconstruction of this object.

We applied our approach to a number of other objects. Fig. 9 shows the result of a hammer, whose handle is axial symmetric and whose head is plane reflection symmetric. Once again, both primary symmetries are identified with the associated domains, and the object is successfully reconstructed.

A final experiment involved a challenging object; the puppet shown in Fig. 10. This object possesses no global symmetries. However, its nine components are all axial symmetric. To achieve the result in Fig.10c, we restricted our search exclusively to axial symmetries. Our approach correctly identifies the major parts of the object, along with the associated symmetries. Through these symmetries, almost all of the occluded shape is successfully reconstructed.

The processing time for all these results fell between 30 sec and 5 min on a low-end PC, depending on the symmetries found. The time depends on the number of symmetries considered by our search algorithm, and is longest for objects without symmetry. The number of points in our data varied between $2{\cdot}10^5$ and $6{\cdot}10^5$.

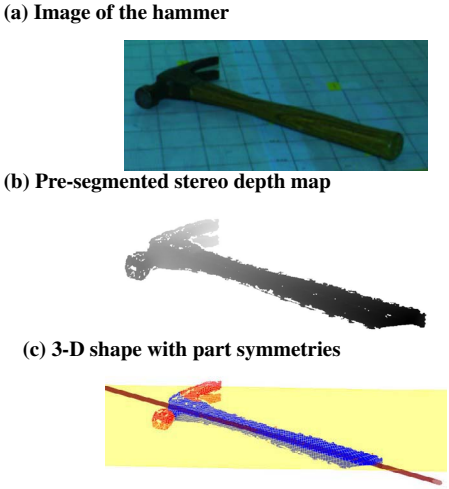

Figure 9. This hammer possesses two symmetries: a local axial symmetry (handle) and a global plane reflection symmetry. Our algorithm correctly identifies these symmetries, and segments the object accordingly. Through these symmetries, it is able to reconstruct the full 3-D shape from a single view.

7. Related Work

Related work on 3-D shape reconstruction was already reviewed in the introduction to this paper. The geometry and topology of symmetries is extensively discussed in [14, 21].

Beyond the context of 3-D shape recovery, The idea of using symmetry is not entirely new to the field of computer vision. In 2-D vision, techniques in [16, 9] describe how symmetries may be detected in 2-D images. The work in [22] finds symmetries in 2-D images and uses those symmetries to improve reconstructions of visible features in structure from motion. The papers [19, 20] reconstruct objects having a generalized axial symmetry from 2-D data using manual initialization; in [20], multiple sets of 2-D data are used to obtain 2-D outlines from multiple viewpoints. [2] shows how 2-D symmetries and anti-symmetries may be used to plan grasps in robot motion planning of planar objects by grasping around the rim. However, techniques based on 2-D images can make only limited use of symmetries to perform 3-D reconstructions. This is because a 2-D reflection distorts 3-D symmetries. Accordingly, the relationship between a 3-D symmetry of an object and the observed reflected 2-D image is complex and subject to ambiguity. Hence, research considering 2-D images does not address the problems solved here.

There has been less work on the topic of symmetry in 3-D data. A paper by Sun and Sherrah [18] describes how certain 3-D symmetries that are global to an object may be detected by converting the problem to the correlation of a Gaussian image. A related paper [23] defines a continuous symmetry measure to quantify the symmetry of both 2-D and 3-D objects; the paper applies this measure to finding the orientation of 3-D symmetries, but does not address object com-

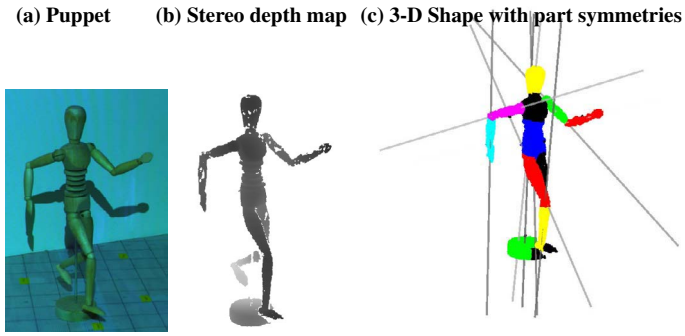

Figure 10. Image of a complex object; stereo depth map; 3-D reconstruction through local axial symmetries.

pletion from incomplete data. Another paper [7] describes how symmetries that are global to an object can be detected in a 3-D voxel model of the object. In [8], the authors apply this idea to the problem of shape retrieval from a database. None of these papers addresses the problem of reconstructing occluded 3-D surfaces from 3-D data.

8. Conclusion

We presented a technique for reconstruction the 3-D surface shape from incomplete 3-D views using symmetries. The "shape from symmetry" algorithm identifies object symmetries from a 3-D range scan of an unknown object, and uses said symmetries for 3-D shape reconstruction. It requires no prior model or database of object shapes. Instead, it analyzes objects for eight common symmetry types. Experimental results show that symmetries can be found for a great number of common objects.

There exist a number of possible extensions. Chief among them is an extension of the space of symmetry types with, for example, translation symmetries (see [14, 21] for a more complete discussion of symmetry types). While the present approach rejected the use of any parametric surface models, using such models may aid in the search process, by restricting the location of possible symmetry features. One might also consider surface normals in the symmetry search, although in our own experiments such information was not found to improve the overall performance of the algorithm. Finally, one could use texture information in the symmetry search, not just shape.

We hope that this paper opens a new direction in the quest for 3-D shape reconstruction. We believe that for many common objects, a single view is sufficient to determine the shape of the object, to the extent required by many practical applications. We hope that future research will lead to improved techniques to exploit object regularities to extrapolate visible surfaces into the occluded regions.

References

[1] P. Besl and N. McKay. A method for registration of 3d shapes. *PAMI*, 14(2):239–256, 1992.
[2] A. Blake, M. Taylor, and A. Cox. Grasping visual symmetry. ICCV-93.
[3] A. Criminisi, I. Reid, and A. Zisserman. Single view metrology. ICCV-99.
[4] B. Horn and M. Brooks, editors. *Shape From Shading*. MIT Press, 1989.
[5] A. E. Johnson and M. Hebert. Using spin images for effi cient object recognition in cluttered 3d scenes. *PAMI*, 21(5):433–449, 1999.
[6] T. Kanade. Recovery of the three-dimensional shape of an object from a single view. *AI*, 17(1-3):409–460, 1981.
[7] M. Kazhdan, B. Chazelle, D.P. Dobkin, A. Finkelstein, and T.A. Funkhouser. A reflexive symmetry descriptor. ECCV-02.
[8] M. Kazhdan, T. Funkhouser, and S. Rusinkiewicz. Symmetry descriptors and 3d shape matching. In *Eurographics Symposium on Geometry Processing*, 2004.
[9] Y. Liu, R. Collins, and W. Rothfus. Robust midsagittal plane extraction from normal and pathological 3d neuroradiology images. *IEEE TMI*, 20(3):175–192, 2001.
[10] H. Mitsumoto, S. Tamura, K. Okazaki, N. Kajimi, and Y. Fukui. 3-D reconstruction using mirror images based on a plane symmetry recovery method. *PAMI*, 14(9):941–946, 1992.
[11] S. Nayar and S. Narasimhan. Vision in bad weather. ICCV-99.
[12] T. Poggio and T. Vetter. Recognition and structure from one 2d model view: Observations on prototypes, object classes and symmetries. A.I. Memo No. 1347, MIT, 1992.
[13] M. Pollefeys, R. Koch, and L. V. Gool. Self-calibration and metric reconstruction in spite of varying and unknown internal camera parameters. ICCV-98.
[14] J. Rosen. *Symmetry Discovered: Concepts and Applications in Nature and Science*. Cambridge University Press, 1975.
[15] S. Rusinkiewicz and M. Levoy. Effi cient variants of the ICP algorithm. 3DIM-01.
[16] D. Shen, H. H. Ip, K. K. Cheung, and E. K. Teoh. Symmetry detection by generalized complex (gc) moments: A close-form solution. *PAMI*, 21(5), 1999.
[17] S. Soatto and R. Brockett. Optimal structure from motion: Local ambiguities and global estimates. CVPR-98.
[18] C. Sun and J. Sherrah. 3d symmetry detection using the extended gaussian image. *PAMI*, 19(2):164–169, 1997.
[19] D. Terzopoulos, A. Witkin, and M. Kass. Symmetry-seeking models and 3D object reconstruction. *Computer Vision*, 1(3):211–221, 1987.
[20] D. Terzopoulos, A. Witkin, and M. Kass. Constraints on deformable models: Recovering 3D shape and nonrigid motion. *AI*, 36:91–123, 1988.
[21] H. Weyl. *Symmetry*. Princeton University Press, 1952.
[22] H. Zabrodsky and D. Weinshall. Using bilateral symmetry to improve 3D reconstruction from image sequences. *CVIU*, 67(1):48–57, 1997.
[23] R. Zabrodsky, S. Peleg, and D. Avnir. Symmetry as a continuous feature. *PAMI*, 17(12):1,154–1,166, 1995.
[24] S. Zucker. Region growing: Childhood and adolescence. *Comput. Graphics Image Processing*, 5:382–399, 1976.